# Additive Point Source Localization (APSL)

T.H.Y Joshi[1], D. Hellfeld[2], M.S. Bandstra[1], R.J. Cooper[1], K. Vetter[1,2]

[1]Nuclear Science Division, Lawrence Berkeley National Laboratory, Berkeley, CA 94720, USA
[2]Department of Nuclear Engineering, University of California, Berkeley, Berkeley, CA 94720, USA

## Introduction

Gamma-ray imaging attempts to reconstruct the spatial and intensity distribution of gamma-emitting radionuclides from a set of measurements. This technique is employed for activities ranging from medical imaging to nuclear security. In many cases this problem is solved by discretizing the spatial dimensions and employing some variant of the Maximum Likelihood Expectation Maximization (MLEM) algorithm. While the generality of this formulation enables use in a wide variety of scenarios, it is also susceptible to overfitting and limited by the discretization of spatial coordinates. We present a novel approach to gamma-ray image reconstruction for scenarios where sparsity may be assumed, for example radiological source search. In this work we formulate point-source localization (PSL) as an optimization problem where both position and intensity are continuous variables. We then extend this formulation and describe an iterative algorithm, additive point-source localization (APSL), for sparse image reconstruction. Finally, we consider a set of simulated source search scenarios and compare APSL with MLEM in terms of image quality and computational efficiency, finding improved accuracy and reduced computational burden with APSL.

## Poisson Likelihood and MLEM

Gamma-ray measurements are governed by Poisson statistics. The negative log-likelihood of a set of $i$ measurements $\mathbf{x}^{[i\times 1]} = [x_0, x_1, \ldots, x_i]^T$ from mean-rates $\boldsymbol{\lambda}^{[i\times 1]} = [\lambda_0, \lambda_1, \ldots, \lambda_i]^T$ is

$$\ell(\mathbf{x}|\boldsymbol{\lambda}) = [\boldsymbol{\lambda} - \mathbf{x} \odot \log \boldsymbol{\lambda} + \log[\Gamma(\mathbf{x}+1)]]^T \cdot \mathbf{1}\,, \tag{1}$$

where $\odot$ denotes element-wise multiplication. The system matrix $\mathbf{V}^{[i\times k]}$ describes the geometric and detector efficiency of the $i$ measurements relative to $k$ image voxels with intensities $\mathbf{w}^{[k\times 1]} = [w_0, \ldots, w_k]^T$. The mean-rates $\boldsymbol{\lambda}$ are the forward-projection of the voxel intensities

$$\boldsymbol{\lambda} = \mathbf{V} \cdot \mathbf{w} + b\boldsymbol{t}\,, \tag{2}$$

where $b$ is a constant background rate and $\boldsymbol{t}^{[i\times 1]}$ are measurement time durations. Maximum Likelihood Expectation Maximization (MLEM) [1, 2] is an iterative algorithm that minimizes Eq. 1. Without background, the update equation is

$$\mathbf{w}^{(j+1)} = \frac{\mathbf{w}^{(j)}}{\boldsymbol{\varsigma}} \odot \mathbf{V}^T \cdot \frac{\mathbf{x}}{\mathbf{V}\cdot\mathbf{w}^{(j)}}\,, \tag{3}$$

where the sensitivity $\boldsymbol{\varsigma}^{[k\times 1]} = \mathbf{V}^T \cdot \mathbf{1}$. This approach is statistically founded and highly general, but can result in overfitting in sparse and underdetermined scenarios. Furthermore, the calculation of $\mathbf{V}$ can be computationally expensive and memory intensive when $k \gg 1$.

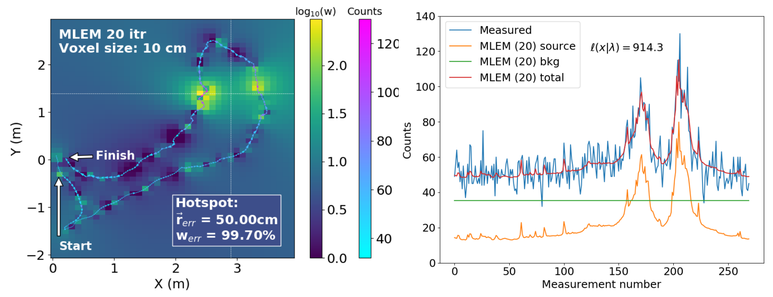


Fig. 1. MLEM reconstructed $\mathbf{w}$ of point source (crosshair) with single non-directional detector along path (left). Comparison of $\mathbf{x}$ and $\hat{\boldsymbol{\lambda}}$ (right).

## Point Source Localization

Under the point-source assumption, the optimal background rate and point-source intensities for each voxel can be solved using MLEM by replacing $\boldsymbol{\lambda} \Rightarrow \boldsymbol{\Lambda}^{[i\times k]} = [\boldsymbol{\lambda}_1, \ldots, \boldsymbol{\lambda}_k]$, $\mathbf{w} \Rightarrow \mathbf{W}^{[k\times k]} = \mathrm{diag}(\mathbf{w})$, $\mathbf{x} \Rightarrow \mathbf{X}^{[i\times k]} = [\mathbf{x}, \ldots, \mathbf{x}]$, $b \Rightarrow \boldsymbol{b}^{[1\times k]} = [b_1, \ldots, b_k]$, and $\boldsymbol{t} \Rightarrow \boldsymbol{T}^{[i\times k]} = [\boldsymbol{t}, \ldots, \boldsymbol{t}]$. Eq. 2 then becomes

$$\boldsymbol{\Lambda} = \mathbf{V}\cdot\mathbf{W} + \boldsymbol{b} \odot \boldsymbol{T}. \tag{4}$$

An analytical solution exists in the absence of background: $\mathbf{W} = \mathbf{X}^T\cdot\mathbf{1}/\mathbf{V}^T\cdot\mathbf{1}$. The voxel in discrete space that alone best describes the data may then be identified with Eq. 1. Note that Eqs. 3 and 4 can be refactored for computational efficiency.

The minimization of Eq. 1 can also be reformulated as an optimization problem not only in intensity, but also in the continuous 3D spatial coordinates of the point-source ($\vec{r_s}$)

$$\underset{(w_s, \vec{r_s}, b)}{\operatorname{argmin}}\ \ell(\mathbf{x}|w_s, \vec{r_s}, b)\,, \tag{5}$$

$$\lambda_i = v_{is} w_s + b t_i\,, \tag{6}$$

$$v_{is} = \eta(\vec{r_s}, \vec{r_i}) t_i / |\vec{r_i} - \vec{r_s}|^2\,. \tag{7}$$

where $\eta$ is the detector's angular response. The response is calculated only where needed, removing the need to compute $\mathbf{V}$. Note that Eq. 5 is no longer convex, but non-convex optimization methods can be used [3].

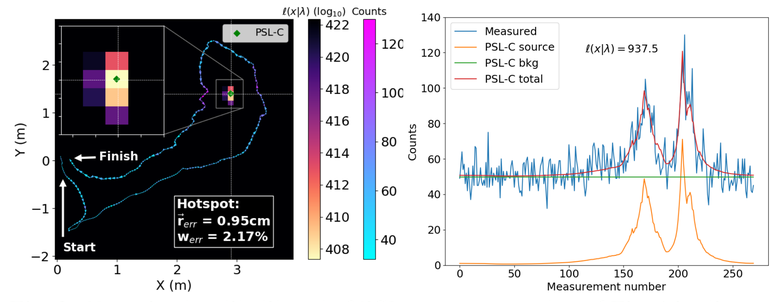


Fig. 2. Negative log-likelihood of PSL reconstructed $\mathbf{w}$ of Fig. 1 in discrete (20 itr) and continuous space (C) (left). Comparison of $\mathbf{x}$ and $\hat{\boldsymbol{\lambda}}$ (right).

## APSL Algorithm

The additive nature of Poisson variables facilitates the inclusion of $m$ known, constant source rate contributions into Eq. 6

$$\lambda_i = v_{is} w_s + \sum_{h=0}^{m-1} v_{ih} w_h + b t_i\,. \tag{8}$$

Now Eq. 5 can be reformulated to localize an additional source

$$\underset{(w_s, \vec{r_s}, b)}{\operatorname{argmin}}\ \ell(\mathbf{x}|w_s, \vec{r_s}, b, \sum_{h=0}^{m-1} v_{ih} w_h)\,. \tag{9}$$

We propose Algorithm 1 to reconstruct a sparse parametric image, $\mathbf{S} = \{(w_0, \vec{r_0}), \ldots, (w_n, \vec{r_n}); \boldsymbol{b}\}$. After each new source is identified, the re-optimization of source positions and intensities can be done in two ways:

1. In the fashion of [3], alternate between
   - Fix intensities and re-optimize positions using conventional optimization methods.
   - Fix positions and re-optimize intensities using MLEM.
2. Re-optimize source positions using conventional optimization methods in optimal intensity space.

**Algorithm 1.** Additive Point Source Localization

```
Initialize reconstruction. S = {(); b}
Solve Eq. 5, append to S
while not converged (Poisson deviance) do
    S_old = S
    Solve Eq. 9 for additional source, append to S
    Re-optimize source positions and intensities, update S
    Test for acceptance of S relative to S_old using AIC [4] or BIC [5]
    if accepted then
        Clean S: drop low weight or weakly contributing sources
        and collapse nearby sources
        Re-optimize current state of source positions and
        intensities, update S
    else
        S = S_old
        converged = True
```

## Results

The performance of the APSL algorithm is demonstrated using a simulated single non-directional detector with an effective area of 6.5 cm$^2$. While a single detector is used here, APSL is extendable to multi-detector systems with complex response functions. A contextual sensor package was used for Simultaneous Localization and Mapping (SLAM) - producing a 3D point cloud of the surrounding environment and tracked position and orientation information at 10 Hz. A SLAM system was used because it was readily available, though it is not required with a non-directional detector (GPS or similar would suffice). A path with a total of 1750 poses was collected over $\tilde{1}75$ sec. Four synthetic point-sources with activities ranging from 25-75 $\mu$Ci were injected into a mean background rate of 12 cps throughout the path at standoffs from 1-2 m at closest approach. The 3D imaging results (top-down) are shown in Fig. 3 and the APSL reconstruction errors in Table I. Sample runtime performance results are shown in Table II.

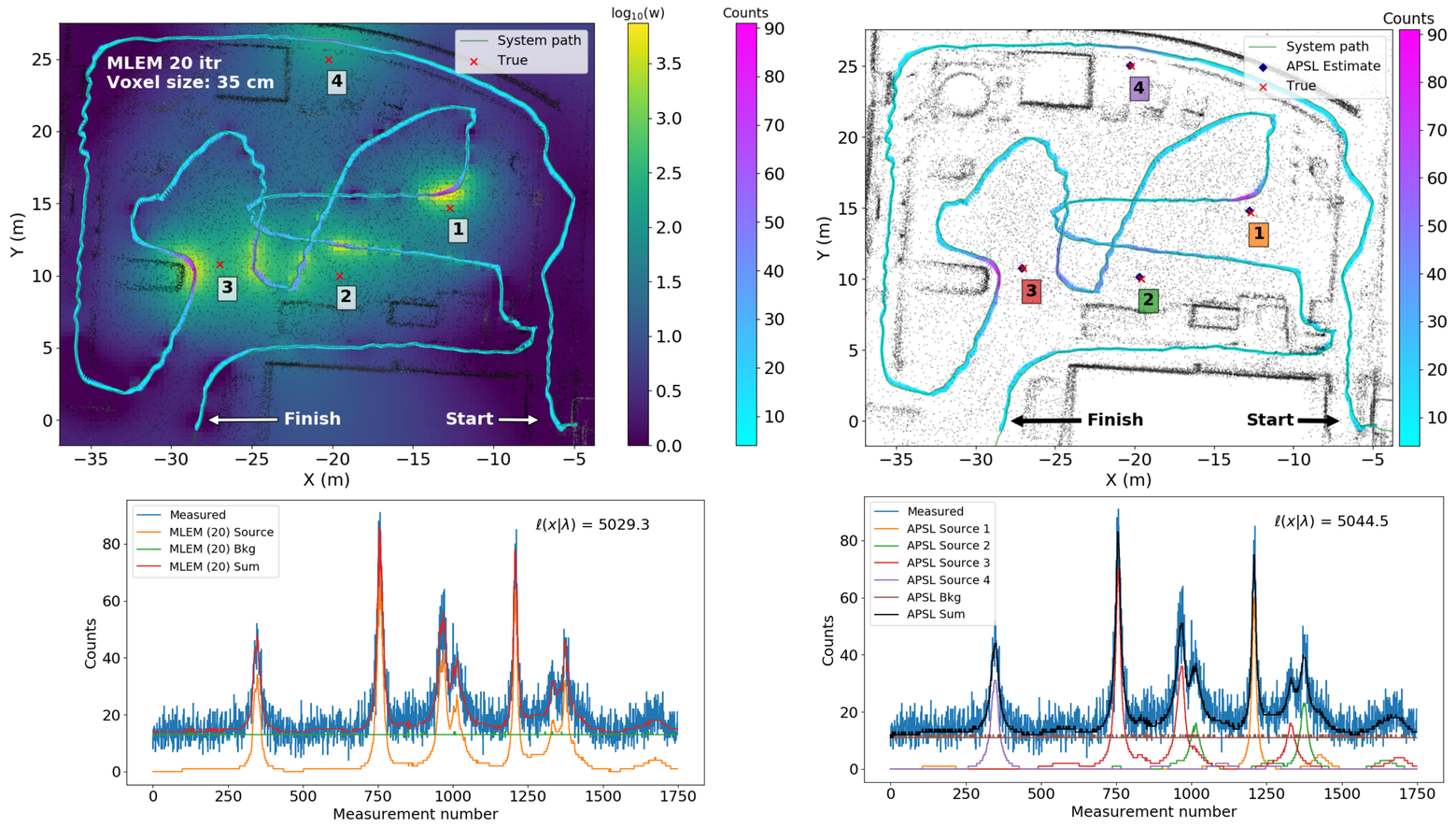


Fig. 3. Multiple point-source image reconstruction using MLEM (top left) and APSL (top right) using a simulated single non-directional detector. Synthetic source counts were injected into a background rate of 12 cps. Comparison of $\mathbf{w}$ and $\hat{\boldsymbol{\lambda}}$ using MLEM (bottom left) and APSL (bottom right).

APSL shows a clear improvement over MLEM in both localization and quantification of each individual source activity. APSL also clearly fits four unique sources while MLEM results in diffuse hotspots biased towards the path as well as high frequency noise throughout the image.

Table I. APSL reconstruction errors.

| | Source 1 | Source 2 | Source 3 | Source 4 |
|---|---|---|---|---|
| $\mathbf{w}_{\mathrm{true}}$ ($\mu$Ci) | 25.4 | 40.8 | 74.9 | 47.0 |
| $\hat{\mathbf{w}}_{\mathrm{err}}$ (%) | 17.2 | 7.4 | 13.9 | 6.5 |
| $\vec{\boldsymbol{r}}_{\mathrm{err,XY}}$ (cm) | 13.2 | 20.4 | 8.4 | 9.1 |
| $\vec{\boldsymbol{r}}_{\mathrm{err,Z}}$ (cm)$^\dagger$ | 74.6 | 39.0 | 63.2 | 264.9 |

$^\dagger$ Generally, $\vec{\boldsymbol{r}}_{\mathrm{err,Z}} > \vec{\boldsymbol{r}}_{\mathrm{err,XY}}$ due to the non-directional detector used and that the path primarily moved in XY, without much change in Z.

## Runtime Comparison

Table II. Sample runtime performance of reconstruction algorithms on 2.7 GHz Intel Core i7 4-core CPU.

| Method | $N_{\mathrm{voxels}}$ | $N_{\mathrm{poses}}$ | $N_{\mathrm{srcs}}$ | Itr | Time (s) | Fig. |
|---|---|---|---|---|---|---|
| MLEM | $8\times10^4$ | 270 | 1 | 20 | $12.9^a + 1.0^b$ | 1 |
| PSL | $8\times10^4$ | 270 | 1 | 20 | $12.9^a + 36.8^b$ | 2 |
| APSL | - | 270 | 1 | - | $0.2^b$ | 2 |
| MLEM | $9.6\times10^4$ | 1750 | 4 | 20 | $87.3^a + 8.1^b$ | 3 |
| APSL | - | 1750 | 4 | - | $19.5^b$ | 3 |

[a] system matrix, [b] reconstruction

## Summary

- MLEM suffers from overfitting in sparse scenarios.
- Introducing the point source assumption in discretized space yields improved performance relative to MLEM, at the expense of reconstruction time.
- Solving PSL as an optimization over continuous intensity and position space increases localization accuracy and computational efficiency.
- We propose APSL for sparse parametric image reconstruction, showing improved accuracy and reduced computational burden over MLEM
- APSL is easily extendable to multi-detector systems with complex response functions.
- Future work includes: streaming operation, multi-energy reconstruction, point cloud constraints, continued improvements to computational efficiency, variable background.

## References

[1] A. P. Dempster, N. M. Laird, and D. B. Rubin, "Maximum Likelihood from Incomplete Data via the EM Algorithm," *J. of the Royal Statistical Society, Series B*, vol. 39, no. 1, pp. 1–38, 1977.

[2] L. A. Shepp and Y. Vardi, "Maximum Likelihood Reconstruction for Emission Tomography," *IEEE Trans. on Medical Imaging*, vol. 1, no. 2, pp. 113–122, 1982.

[3] N. Boyd, G. Schiebinger, and B. Recht, "The Alternating Descent Conditional Gradient Method for Sparse Inverse Problems," *SIAM J. Optim.*, vol. 27, no. 2, pp. 616–639, 2017.

[4] H. Akaike, "A New Look at the Statistical Model Identification," *IEEE Trans. on Auto. Control*, vol. 19, no. 6, pp. 716–723, 1974.

[5] G. Schwarz, "Estimating the Dimension of a Model," *The Annals of Statistics*, vol. 6, no. 2, pp. 461–464, 1974.

## Contact

**Daniel Hellfeld**

*PhD Candidate* | UC Berkeley | Department of Nuclear Engineering
*Graduate Research Fellow* | Nuclear Science and Security Consortium
Email: dhellfeld@berkeley.edu | Web: dhellfeld.github.io

**IEEE NSS-MIC - Sydney, Australia**
10-17 November 2018

*This material is based on work supported by the Department of Energy National Nuclear Security Administration through the Nuclear Science and Security Consortium under Award No. DE-NA0000979. This support does not constitute an express or implied endorsement on the part of the United States Government.*